Strong magnetic coupling of an inhomogeneous nitrogen-vacancy ensemble to a cavity

K. Sandner,[1] H. Ritsch,[1] R. Amsüss,[2] Ch. Koller,[2,3] T. Nöbauer,[2] S. Putz,[2,3] J. Schmiedmayer,[2] and J. Majer[2,3]

[1]*Institute for Theoretical Physics, Universität Innsbruck, Technikerstrasse 25, 6020 Innsbruck, Austria*

[2]*Vienna Center for Quantum Science and Technology, Atominstitut, TU-Wien, 1020 Vienna, Austria*

[3]*Center for Micro- and Nanostructures ZNMS, TU Wien, 1040 Vienna, Austria*

(Received 2 January 2012; published 7 May 2012)

We study experimentally and theoretically a dense ensemble of negatively charged nitrogen-vacancy centers in diamond coupled to a high-Q superconducting coplanar waveguide cavity mode at low temperature. The nitrogen-vacancy centers are modeled as effective spin-one defects with inhomogeneous frequency distribution. For a large enough ensemble the effective magnetic coupling of the collective spin dominates the mode losses and inhomogeneous broadening of the ensemble and the system exhibits well-resolved normal-mode splitting in probe transmission spectra. We use several theoretical approaches to model the probe spectra and the number and frequency distribution of the spins. This analysis reveals an only slowly temperature-dependent q-Gaussian energy distribution of the defects with a yet unexplained decrease of effectively coupled spins at very low temperatures below 100 mK. Based on the system parameters we predict the possibility to implement an extremely stable maser by adding an external pump to the system.

DOI: 10.1103/PhysRevA.85.053806 PACS number(s): 42.50.Pq, 42.50.Ct, 61.72.jn, 03.67.−a

I. INTRODUCTION

Systems of spin ensembles coupled to a cavity mode are considered a promising physical realization for processing and storage of quantum information [1], ultrasensitive high-resolution magnetometers [2], or localized field probes. Collective magnetic coupling of a large ensemble to the field mode allows us to reach the strong-coupling regime, even if a single particle is hardly coupled. Implementations based on superconducting coplanar waveguide (CPW) resonators provide an interface of the spin ensemble with processing units for superconducting qubits. Here the spins can serve as a quantum memory or as a bridge to optical readout and communication [3].

Different types of ensembles were proposed for this setup, ranging from clouds of ultracold atoms [3] over polar molecules [4] to solid-state systems like rare-earth spin ensembles [5] or color centers in diamond [6,7]. Here we focus on the negatively charged nitrogen-vacancy (NV) defects in diamond. Those are naturally present in diamond but can also be readily engineered with very high densities, still maintaining long lifetimes and slow dephasing in particular at low temperatures of $T < 1$ K. In the optical domain, they are extremely stable and have been very well studied for many years [8].

The magnetic properties of the relevant defect states can be conveniently modeled by effective independent spin-one particles, where the effective local interaction of the electrons within the defect shifts the $(m_S = \pm 1)$ states with respect to the $m_S = 0$ state [9]. On the one hand, this coupling provides the desired energy gap in the 3-GHz regime, but, on the other hand, as a consequence of local variations of the crystal field, this shift exhibits a frequency distribution leading to an inhomogeneous broadening of the ensemble. The inhomogeneities are thought to be predominantly caused by crystal strain and excess nitrogen, which is not paired with a neighboring vacancy [10].

While, for a perfectly monochromatic ensemble of N particles in a cavity, strong coupling simply requires an effective coupling $g_{\text{single}}\sqrt{N}$ larger than the cavity and spin decay rates, not only the width, but also the details of the inhomogeneous distribution are known to strongly influence the dynamic properties of the real world system [11–13]. In particular, Gaussian and Lorentzian distributions of equal half widths lead to different widths and magnitudes of the vacuum Rabi splitting. Only above a critical coupling strength the rephasing via common coupling to the cavity mode will prevent dephasing of the collective excitation and lead to a well-resolved vacuum Rabi splitting.

In our theoretical studies we use different approximation levels to analyze the central physical effects present in the coupled system of cavity and inhomogenously broadened ensemble, as they are observed in the measurements. While many qualitative features can be readily understood from a simple, coupled damped oscillator model with an effective linewidth, a detailed understanding of the observed frequency shifts and coupling strengths in the experiments requires more sophisticated modeling of the energy distributions and dephasing mechanisms. In particular the observed temperature dependence relies on a finite temperature master-equation treatment of a collective spin with proper dephasing terms. This is compared to the experimental values of up to $N \approx 10^{12}$ particles as presented already in [7]. We focus on the interplay between the cavity mode and the ensemble and in particular on the role of the frequency distribution of the ensemble. This analysis is also applicable to systems other than NV ensembles. Though the detailed microscopic mechanisms within the NV ensemble that cause the inhomogeneous frequency distribution are of considerable relevance, our central point of interest is the effect of the inhomogeneity rather than its origin. A thorough investigation of the broadening mechanisms is beyond the scope of this manuscript.

The paper is organized as follows. The general properties of the system are introduced in Sec. II. A first approximative treatment using coupled harmonic oscillators is shown in Sec. III A. In Sec. III B we incorporate the inhomogeneous frequency distribution of the NVs via an extra decay of the polarization of the ensemble. In this context we also analyze the effects of thermal excitations in the spin ensemble and in

the cavity. Finally, in Sec. III C we interpret our measurements using the resolvent formalism in order to extract the exact form of the inhomogeneity [13]. The prospect of implementing a narrow bandwidth transmission line micromaser using an inhomogenously broadened ensemble is discussed in Sec. IV.

II. GENERAL SYSTEM PROPERTIES AND EXPERIMENTAL IMPLEMENTATION

The ground state of the NV center is a spin triplet ($S = 1$), where the $m_S = \pm 1$ states are split from the $m_S = 0$ state by about 2.88 GHz at zero magnetic field [10]. In addition the degeneracy between the $m_S = \pm 1$ states is lifted due to the broken C_{3v} symmetry. Applying a homogeneous magnetic field enables Zeeman tuning of the $m_S = \pm 1$ states, so that the $m_S = 0 \rightarrow \pm 1$ transitions can be tuned selectively into resonance with the CPW cavity.

Note that here the Zeeman tuning is also varying with the NV center's orientation relative to the applied field direction. In NV center ensembles all the four symmetry allowed orientations of the NV main axis are found and in general each orientation will enclose a different angle with the magnetic field and will be shifted by a different amount.

However, if the magnetic-field direction is oriented within the (001) plane of the diamond, always two of four orientations exhibit the same angle with the field and at special angles all four are tuned by the same amount.

In general we therefore have to distinguish between the $m_S^{\mathrm{I,II}} = \pm 1$ states of subensemble I and II. The Hamiltonian for one NV subensemble can be written as

$$H_{\mathrm{NV}} = \tilde{g}\mu_B \mathbf{B}\cdot\mathbf{S} + DS_z^2 + E\left(S_x^2 - S_y^2\right), \qquad (1)$$

where the first term describes the Zeeman effect with $\tilde{g} = 2$ for an NV center and μ_B is the Bohr magneton. The second term denotes the zero-field splitting with $D = 2.88$ GHz and typical strain-induced E parameters of several MHz. The presence of nonzero E parameters in large NV ensembles causes a mixing of the pure Zeeman states for low magnetic-field values which are denoted as $|0,\pm\rangle$. As the magnetic-field amplitude is increased, the eigenstates are again well approximated by pure Zeeman states.

The transition frequencies $\omega_{\pm}^{\mathrm{I,II}}$ between the eigenstates $|0\rangle_{\mathrm{I,II}}$ and $|\pm\rangle_{\mathrm{I,II}}$ are depicted in Fig. 1(b).

A. Theoretical model

Assuming that only the transition $|0\rangle_{\mathrm{I}} \rightarrow |-\rangle_{\mathrm{I}}$ with frequency ω_-^{I} is in or close to resonance with the cavity mode, we can reduce the description of a single NV to a two-level system. The effects caused by the presence of the far detuned $|+\rangle_{\mathrm{I}}$ state can be included in a constant effective frequency shift as addressed in Sec. III A. We thus approximate the composed system of cavity and ensemble with the Tavis-Cummings Hamiltonian:

$$H_{\mathrm{TC}} = \omega_c a_c^{\dagger} a_c + \frac{1}{2}\sum_j^N \omega_j \sigma_j^z + \sum_j^N (g_j \sigma_j^{+} a_c + \mathrm{H.c.}), \qquad (2)$$

where $\hbar = 1$. The first two terms describe the unperturbed energies of the cavity, with frequency ω_c and creation operator $a_c^{\dagger}$, and of the N ensemble spins using the usual Pauli spin operators $[\sigma_i^{+},\sigma_j^{-}] = \sigma_i^z \delta_{ij}$. Each spin can have a different frequency ω_j which is statistically spread around the center frequency ω_-^{I}. The third term describes the coupling to the cavity with individual strength g_j. Assuming that the ensemble spins are confined to a volume that is small compared to the wavelength, the ensemble will interact collectively with the mode. In the case of few excitations, the ensemble behaves like a harmonic oscillator which couples to the mode with the collective coupling strength Ω. The collective coupling strength is given by $\Omega = \sqrt{\sum_j^N |g_j|^2}$, which for identical $g_j = g_{\mathrm{single}} = g$ gives $\Omega = g\sqrt{N}$. The effects of unequal coupling of the spins are addressed in [14]. To include the probe field of the cavity we add another term, $H_p = i(\eta a_c^{\dagger} e^{-i\omega_p t} - \eta^* a_c e^{i\omega_p t})$, to Eq. (2).

Effects of the coupling to a finite temperature bath are analyzed in Sec. III B, where we study the master equation of the ensemble-cavity system.

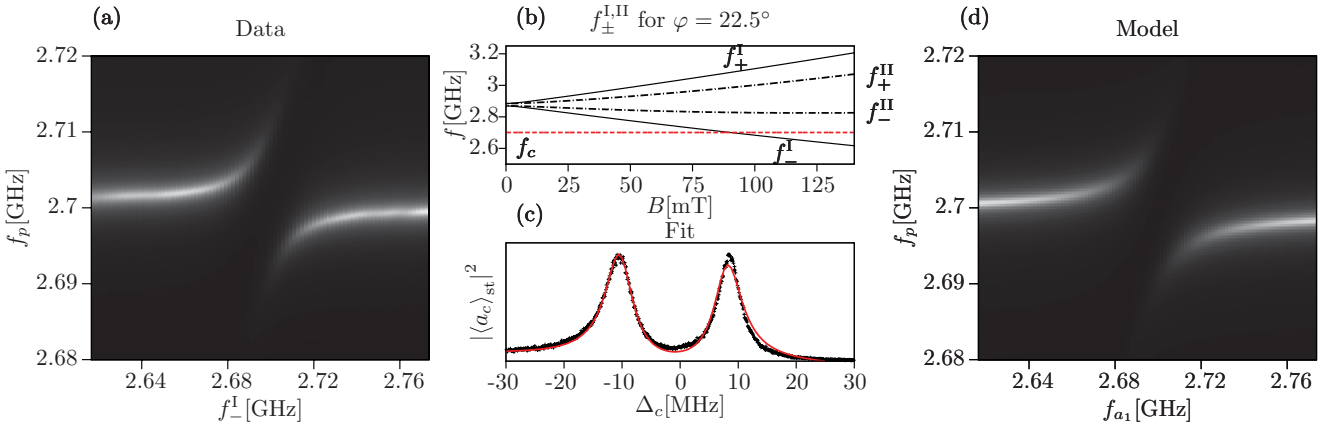

FIG. 1. (Color online) (a) Measured transmission as a function of $f_-^{\mathrm{I}} = \omega_-^{\mathrm{I}}/(2\pi)$ tuned by the magnetic field and pump frequency $f_p = \omega_p/(2\pi)$. (b) Transition frequencies $f_\pm^{\mathrm{I,II}} = \omega_\pm^{\mathrm{I,II}}/(2\pi)$ as a function of the magnetic field for a field angle of $\varphi = 22.5^{\circ}$. The frequency of the cavity $f_c = \omega_c/(2\pi)$ is denoted by the (red) dashed line. (c) Fit of $|\langle a_c\rangle_{\mathrm{st}}|^2$ to the transmitted signal close to the resonance. We obtain the decay rate $\gamma = 10.92$ MHz. (d) $|\langle a_c\rangle_{\mathrm{st}}|^2$ as a function of f_{a_1} and f_p incorporating the parameters obtained from the fit.

For an ensemble with identical frequencies and coupling strengths we find that we can reach the regime of coherent oscillations between the cavity and the ensemble spins if the collective coupling Ω dominates the linewidth of the cavity κ and the decay rate of the single spin $\gamma_{\rm hom}$. This is commonly known as the strong-coupling regime. In the case of an ensemble with inhomogeneous frequency distribution it is not immediately clear under which conditions we can observe the avoided crossing. Here we address the influence of the width and form of the inhomogeneous frequency distribution on the avoided crossing.

B. Experimental setup and parameters

The experimental setup has been described already in detail in [7] and is explained here only in brevity in the following. The heart of the experiment is a $\lambda/2$ superconducting coplanar waveguide (CPW) resonator with a center frequency of 2.7 GHz that is cooled down to 20 mK in a dilution refrigerator. In order to couple NV defect centers to the microwave field in the cavity, a (001)-cut single-crystal diamond is placed in the middle of the resonator, where the oscillating magnetic field exhibits an antinode. A meander geometry of the resonator ensures that a large fraction of the magnetic mode volume is covered by spins. The high-pressure high-temperature diamond chosen in this setup contains an NV concentration of about 6 ppm, which corresponds to an average separation of about 10 nm.

A two-axis Helmholtz coil configuration creates a homogeneous static magnetic field oriented with an arbitrary direction within the (001) plane of the diamond, which is at the same time parallel to the resonator chip surface. Since perpendicular magnetic-field components with respect to the resonator surface would shift the resonance frequency of the cavity, great care was taken during the alignment of the setup. With the diamond on top of the chip the cavity quality factor is $Q = 3200$.

In a typical experiment, we first set the magnetic-field direction and amplitude and then measure the microwave transmission through the cavity with a vector network analyzer.

III. CAVITY TRANSMISSION SPECTRA FOR INHOMOGENEOUS ENSEMBLES

As a generic experiment to test and characterize the system properties we analyze the weak-field probe transmission spectrum through the resonator in the weak-field limit, where the number of excitations is negligible compared to the ensemble size. Hence, at least at low temperatures, we can largely ignore saturation effects and apply various simplified theoretical descriptions to extract the central system parameters. In fact, as we deal with more than $N > 10^{11}$ spins in a transition frequency range of about 10^7 Hz, we have several thousand spins per Hz frequency range and up to a million spins within the homogeneous width of at least several kHz. Hence theoretical modeling as a collection of effective oscillators should provide an excellent model basis. This has to be taken with care at higher temperatures, $k_B T \approx \hbar\omega_c$, when we have a significant fraction of the particles excited.

A. Coupled collective oscillator approximation

A photon that enters the cavity will be absorbed into a symmetric excitation of the ensemble spins with a weight given by the individual coupling strength. Subsequently the broad distribution of the spin frequencies induces a relative dephasing of this excitation so that the backcoupling to the cavity mode is suppressed. As spontaneous decay ($T_1 \approx 44$ s) is negligibly slow [7], the decay rate of the polarization of the ensemble is just proportional to this dephasing and thus the inhomogeneous width of the spins.

As the number of photons entering the ensemble is very small compared to N in a first model, we simply approximate the ensemble as a harmonic oscillator with frequency $\omega_{a1} = \omega^{\rm I}_-$ and an effective large width γ that mimics the inhomogeneity. The ensemble oscillator is coupled to the cavity with frequency ω_c and decay rate κ.

This very simplified model already allows us to study the coupling dynamics of the collective energy levels of the broadened ensemble and the cavity mode, and in particular the avoided crossing of the energy levels, when the relative energies are varied.

To keep the model as simple as possible but still grasping the essential properties, the presence of the other off-resonant spin ensembles at $\omega^{\rm I}_+$, $\omega^{\rm II}_-$, and $\omega^{\rm II}_+$ is modeled by additional oscillators with frequency ω_{aj}, $(j = 2,3,4)$ and equal decay rate γ.

For a small probe field injected into the cavity with the frequency ω_p the corresponding equations in a frame rotating with ω_p then read

$$\frac{d}{dt}\langle a_c\rangle = -(\kappa + i\Delta_c)\langle a_c\rangle - ig\sum_{j=1}^{4} N_j\langle\sigma_j^-\rangle + \eta, \tag{3}$$

$$\frac{d}{dt}\langle\sigma_j^-\rangle = -\left(\frac{\gamma}{2} + i\Delta_{aj}\right)\langle\sigma_j^-\rangle - ig\langle a_c\rangle, \tag{4}$$

with probe amplitude η, $\Delta_c = \omega_c - \omega_p$, and $\Delta_{aj} = \omega_{aj} - \omega_p$. From Eqs. (3) and (4) we can calculate the steady-state field in the cavity $\langle a_c\rangle_{\rm st}$, which can be written as

$$\langle a_c\rangle_{\rm st} = \frac{\eta}{\kappa + \Gamma_a + i(\Delta_c - U_a) + \frac{g^2 N_1}{\gamma/2 + i\Delta_{a1}}}, \tag{5}$$

where

$$\Gamma_a = \sum_{j=2}^{4}\frac{g^2 N_j \gamma/2}{(\gamma/2)^2 + \Delta_{aj}^2} \quad\text{and}\quad U_a = \sum_{j=2}^{4}\frac{g^2 N_j \Delta_{aj}}{(\gamma/2)^2 + \Delta_{aj}^2}. \tag{6}$$

In the absence of the off-resonant levels ($N_2 = N_3 = N_4 = 0$) we recover the situation, where for $\omega_{a1} = \omega_c$ and $g\sqrt{N_1} > (\gamma/2 - \kappa)/2$ we find two normal modes split by $2\sqrt{g^2 N_1 - (\gamma/2 - \kappa)^2/4}$. The off-resonant transitions make the situation more complex. As it can be seen in Eq. (5), they induce a shift U_a of the cavity frequency and increase the decay rate of the cavity by Γ_a. Both shift and additional decay rate depend on the probe frequency ω_p. For the parameters in our measurement we find that Γ_a is negligible compared to κ. We further approximate U_a by setting $\omega_p = \omega_c$ [as the scan range of ω_p around ω_c is small compared to ω_{aj} $(j = 2,3,4)$]. We obtain the model of two coupled oscillators, where one of them has been shifted by the off-resonant transitions. As a function of ω_p and ω_{a1} (tuned by the magnetic field), $|\langle a_c\rangle_{\rm st}|^2$ shows

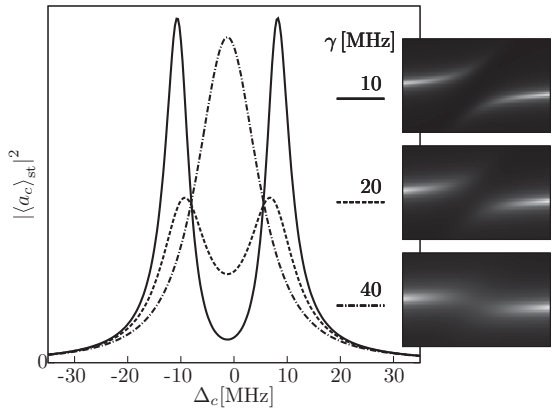

FIG. 2. Simulation of the normal-mode splitting at resonance ($\omega_c - U_a = \omega_{a1}$) for different values of γ. Finally, for large values of γ the doublet is not resolved any more and the avoided crossing (sketched on the right) becomes blurred.

an avoided crossing. Although the off-resonant transitions are shifted by the magnetic field as well, the effect in U_a is negligibly small, so that we assume that U_a is constant.

We show the measured signal at the avoided crossing in Fig. 1(a). By fitting $|\langle a_c\rangle_{st}|^2$ to the normal-mode splitting we can deduce the inhomogeneous width γ and the effective coupling $g\sqrt{N}$. The Q factor of our cavity corresponds to $\kappa/(2\pi) = 0.4$ MHz, then 2κ is the full width at half maximum (FWHM) of the cavity resonance. An exemplary fit result is shown in Fig. 1(c). We have included a linear term in the fit to account for a background in the data. In Fig. 1(d) we plot $|\langle a_c\rangle_{st}|^2$ using the obtained parameters.

From the fit we deduce a decay rate $\gamma = 10.92$ MHz of the ensemble oscillator and an effective coupling of $g\sqrt{N} = 9.51$ MHz. To demonstrate the effect of the ensemble oscillator width γ on the normal-mode splitting, we plot $|\langle a_c\rangle_{st}|^2$ for $\omega_c - U_a = \omega_{a1}$ and different values of γ in Fig. 2.

Treating the ensemble as a broad harmonic oscillator with decay rate γ corresponds to the assumption that the frequency distribution of the real ensemble is a Lorentzian distribution, given that all spins couple with equal strength [13].

B. Polarization decay and collective coupling at finite temperature

Despite the fact that cooling to very low temperatures is possible in the experiments, it is still important and instructive to study the role of thermal excitations in the system. In contrast to previous models based on virtually zero T atomic ensembles, the NV centers are in thermal contact with the chip at small but finite T. We will now investigate how sensitive the system reacts on thermal fluctuations.

At this point we include any shifts caused by the off-resonant ensembles in an effective detuning and concentrate on the collective coupling between the cavity at ω_c and the near resonant ensemble centered around ω_-^{I}. For simplicity we assume equal coupling g for all spins to get

$$\tilde{H}_{\mathrm{TC}} = \omega_c a_c^\dagger a_c + \frac{1}{2}\omega_-^{\mathrm{I}} \sum_j^N \sigma_j^z + g \sum_j^N (\sigma_j^+ a_c + \mathrm{H.c.}). \tag{7}$$

To include thermal excitations of the mode and the ensemble we have to add standard Liouvillian terms to the dynamics and study the corresponding master equation of the reduced cavity-ensemble system [15], where the inhomogeneous width of the ensemble is still simply approximated by an effective dephasing term γ_p for the polarization. In this model decay γ_{hom} and dephasing γ_p are described by separate quantities, which already should improve the model. The master equation reads

$$\frac{d}{dt}\rho = \frac{1}{i}[\tilde{H}_{\mathrm{TC}} + H_p, \rho] + \mathcal{L}[\rho], \tag{8}$$

where

$$\begin{aligned}\mathcal{L}[\rho] = {} & \kappa[\bar{n}(T,\omega_c)+1](2a_c\rho a_c^\dagger - a_c^\dagger a_c\rho - \rho a_c^\dagger a_c) + \kappa\bar{n}(T,\omega_c)(2a_c^\dagger\rho a_c - a_c a_c^\dagger\rho - \rho a_c a_c^\dagger) \\ & + \frac{\gamma_{\mathrm{hom}}}{2}[\bar{n}(T,\omega_-^{\mathrm{I}})+1]\sum_{j=1}^N(2\sigma_j^-\rho\sigma_j^+ - \sigma_j^+\sigma_j^-\rho - \rho\sigma_j^+\sigma_j^-) + \frac{\gamma_{\mathrm{hom}}}{2}\bar{n}(T,\omega_-^{\mathrm{I}})\sum_{j=1}^N(2\sigma_j^+\rho\sigma_j^- - \sigma_j^-\sigma_j^+\rho - \rho\sigma_j^-\sigma_j^+) \\ & + \frac{\gamma_p}{2}\sum_{j=1}^N(\sigma_j^z\rho\sigma_j^z - \rho).\end{aligned} \tag{9}$$

The first two lines of Eq. (9) describe the coupling of the cavity to the bath, while the next two lines include the coupling of the ensemble to the bath. The number of thermal excitations at temperature T and frequency ω is denoted by $\bar{n}(T,\omega)$. The term in the last line introduces nonradiative dephasing at a rate γ_p of the spins and thereby models the inhomogeneity.

Based on the master equation we can derive a hierarchic set of equations for various system expectation values starting with

$$\begin{aligned}\frac{d}{dt}\langle a_c\rangle &= \mathrm{Tr}\left\{a_c\frac{d}{dt}\rho\right\} \\ &= -(\kappa + i\Delta_c)\langle a_c\rangle - igN\langle\sigma_i^-\rangle + \eta,\end{aligned} \tag{10}$$

$$\begin{aligned}\frac{d}{dt}\langle\sigma_i^-\rangle = {} & -\left[\frac{\gamma_{\mathrm{hom}}}{2} + \gamma_{\mathrm{hom}}\bar{n}(T,\omega_-^{\mathrm{I}}) + \gamma_p + i\Delta_-^{\mathrm{I}}\right]\langle\sigma_i^-\rangle \\ & + ig\langle\sigma_i^z a_c\rangle,\end{aligned} \tag{11}$$

$$\frac{d}{dt}\langle\sigma_i^z\rangle = -i2g\left(\langle\sigma_i^+ a_c\rangle - \langle\sigma_i^- a_c^\dagger\rangle\right) - \gamma_{\rm hom}\left(\langle\sigma_i^z\rangle + 1\right) - 2\gamma_{\rm hom}\bar{n}(T,\omega_-^{\rm I})\langle\sigma_i^z\rangle, \quad (12)$$

which also includes equations for $\langle a_c\sigma_i^+\rangle$, $\langle a_c\sigma_i^z\rangle$, $\langle\sigma_i^+\sigma_j^-\rangle$, $\langle a_c^\dagger a_c\rangle$, $\langle a_c\sigma_i^-\rangle$, $\langle a_c^\dagger a_c^\dagger\rangle$, $\langle\sigma_i^-\sigma_j^-\rangle$, $\langle\sigma_i^z\sigma_j^+\rangle$, $\langle\sigma_i^z\sigma_j^z\rangle$, and $\langle a_c^\dagger a_c\sigma_i^z\rangle$. In order to truncate the system higher-order terms in the equations are expanded in a well-defined way [16], then higher-order cumulants are neglected [17,18]. The equations again are written in a frame rotating with the cavity probe frequency ω_p. Despite the inhomogeneous broadening, which is included by the nonradiative dephasing of the spins, we assume that all spins are equal so that we only have to include the equations for one spin i and pairs i,j [17]. This set of equations can be integrated numerically to study the dynamics of the coupled system. We note that when we fix $\langle\sigma_i^z\rangle = -1$ we immediately arrive at the model discussed in Sec. III A with $\gamma = \gamma_{\rm hom} + 2\gamma_p$.

In our experiment we measure the avoided crossing for different temperatures of the environment and compare it to the results of our model. First we note that the steady state of the inversion as a function of the temperature $\langle\sigma_i^z(T)\rangle_{\rm st}$ can be written as [5]

$$\left\langle\sigma_i^z(T)\right\rangle_{\rm st} = \frac{1}{1+2\bar{n}(T,\omega_-^{\rm I})}\left\langle\sigma_i^z(T=0)\right\rangle_{\rm st} = \tanh\left(\frac{\hbar\omega_i}{2k_BT}\right)\left\langle\sigma_i^z(T=0)\right\rangle_{\rm st}. \quad (13)$$

For higher temperatures $\langle\sigma_i^z(T)\rangle_{\rm st}$ is reduced and therefore so are the effective number of NVs that take part in the dynamics. In the model equations this is represented by the last term in Eq. (11) for the polarization involving $\langle a_c\sigma_i^z\rangle$, which leads to a cutoff for the coupling at higher T. As a zero-field approximation we thus write

$$\Omega(T) = g\sqrt{N\tanh\left(\frac{\hbar\omega_-^{\rm I}}{2k_BT}\right)}, \quad (14)$$

where we replaced ω_i by the center frequency $\omega_-^{\rm I}$. Equation (14) should give an approximate description of the reduction of the Rabi splitting with increasing temperature.

This treatment however neglects the presence of the $m_S = +1$ state which will also be populated with increasing T. Including this level and assuming $\bar{n}(T,\omega_+^{\rm I}) \approx \bar{n}(T,\omega_-^{\rm I})$ we find the population difference between the $m_S = 0$ and -1 state to be

$$\frac{N_{-1}(T)}{N} - \frac{N_0(T)}{N} = -\frac{1}{1+3\bar{n}(T,\omega_-^{\rm I})}. \quad (15)$$

This suggests

$$\tilde{\Omega}(T) = g\sqrt{\frac{N}{1+3\bar{n}(T,\omega_-^{\rm I})}} \quad (16)$$

to be a better description for the temperature dependence of the coupling.

In a second step we integrate the whole hierarchic set of equations numerically for $\omega_c = \omega_-^{\rm I}$ and varying pump frequency ω_p. From $|\langle a_c\rangle_{\rm st}|^2(\omega)$ we determine the Rabi splitting

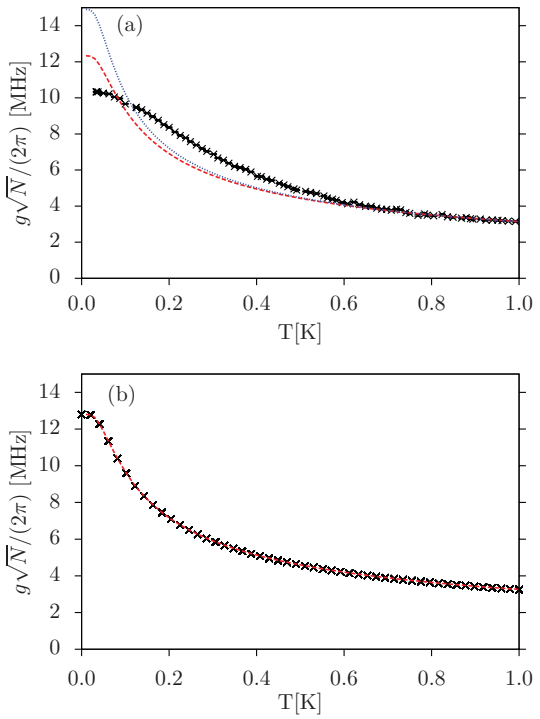

FIG. 3. (Color online) (a) Collective coupling strength obtained from our measurements for different temperatures (black markers) and $\Omega(T) = a_0\{\tanh[\hbar\omega_-^{\rm I}/(2k_BT)]\}^{1/2}$ (red dashed line), where a_0 was chosen to match the high-temperature behavior. Including the $m_S = +1$ state via Eq. (16) gives the result denoted by the blue dotted line. (b) Collective coupling strength determined from the results of the numerical integration of the coupled equations with $g\sqrt{N} = a_0$ [a_0 determined from (a), black markers] and $\Omega(T)$ (red dashed line).

for different temperatures, from which we obtain the collective coupling. This can be compared to our measurements and the approximations in Eqs. (14) and (16).

In Fig. 3(a) we show that the measured coupling strength is in disagreement with the Eq. (14), which is most significant for very low temperatures. Both functions Eqs. (14) and (16) fail to capture the behavior for low temperatures. The disagreement is even more pronounced as we include the effect of the $m_S = +1$ state. So far we have found no definite explanation for the disagreement. However, one possible explanation would be that for low temperatures not all defects are "active." As temperature increases, more NVs become available but at the same time the number of NVs taking part in the dynamics is proportional to $\tanh[\hbar\omega_-^{\rm I}/(2k_BT)]$.

The collective coupling strength determined from the numerical integration of the coupled equations, shown in Fig. 3(b), exactly follows Eq. (14). This shows that the assumption $\Omega(T) \propto \langle\sigma_i^z(T)\rangle_{\rm st}$ is reasonable. However, the almost constant value of the coupling strength $\Omega(T)$ found in the experimental data for very low T cannot be explained in the above theoretical model. Interestingly the same behavior is also found in measurements of the dispersive shift of the cavity mode as a function of temperature by the off-resonant spin ensemble at zero magnetic field. As possible explanations one might think of a reduced thermal excitation probability due to spin-spin coupling or an effective reduction of active NV centers close to zero temperature.

C. Detailed modeling and reconstruction of inhomogeneous distributions

The simplified model descriptions discussed above in Secs. III A and III B provided for an analytically tractable and qualitatively correct description of the effect of an inhomogeneous broadening of the ensemble. This also allows us to get a fairly good estimate for the total width of the frequency distribution of the ensemble. However, such an effective width model inherently is connected to the assumption of a Lorentzian shape of the ensemble frequency distribution. In actual crystals such an assumption is not obvious and other distributions of local-field variations and strain distributions are possible as well.

To obtain more accurate information about the distribution we will now use an improved model based on the resolvent formalism to treat the coupling between a central oscillator (the mode) and the spin degrees of freedom [13,19]. Here each frequency class of spins is treated individually. For low temperatures virtually all spins are in the $m_S = 0$ state, i.e., the lower state of our effective two-level system, and their excitation properties can be approximated by a frequency distributed set of oscillators (the Holstein-Primakoff approximation).

We define creation and annihilation operators for the corresponding ensemble oscillators representing a subclass of two-level systems with equal frequency via

$$\sigma_j^z = -1 + 2a_j^\dagger a_j \quad \text{and} \quad \sigma_j^+ = a_j^\dagger \sqrt{1 - a_j^\dagger a_j} \approx a_j^\dagger. \tag{17}$$

The approximation in Eq. (17) is justified as long as the number of excitations in each ensemble is much smaller than the number of spins in this energy region. In our experimental setup this is very well justified and we thus obtain the unperturbed part of the Hamiltonian as

$$H_0' = \omega_c a_c^\dagger a_c + \sum_j^N \omega_j a_j^\dagger a_j \tag{18}$$

and the interaction term as

$$V' = \sum_j^N (g_j a_j^\dagger a_c + g_j^* a_j a_c^\dagger), \tag{19}$$

which constitute $H' = H_0' + V'$. In this section we account for the decay of cavity excitations and the spontaneous decay of the spins by introducing nonzero imaginary parts of the corresponding transition frequencies $\mathrm{Im}\omega_c = -\kappa$ and $\mathrm{Im}\omega_j = -\frac{1}{2}\gamma_{\mathrm{hom}}$ and the resolvent of the Hamiltonian H' is defined as $G(z) = 1/(z - H')$.

Let us consider the state $|\varphi_c\rangle = |1_c, 0, \ldots, 0\rangle$ where we have one photon in the cavity and no excitation in the ensemble.

The matrix element of the resolvent $G_{\mathrm{cc}}(z) = \langle\varphi_c| G(z) |\varphi_c\rangle$ can be written as

$$G_{\mathrm{cc}}(z) = \frac{1}{z - E_c - R_{\mathrm{cc}}(z)}, \tag{20}$$

where we define the matrix element of the level shift operator:

$$R_{\mathrm{cc}}(z) = V_{\mathrm{cc}}' + \sum_{i\neq c} V_{ci}' \frac{1}{z - E_i} V_{ic}' + \sum_{i\neq c}\sum_{j\neq c} V_{ci}' \frac{1}{z - E_i} V_{ij}' \frac{1}{z - E_j} V_{jc}' + \ldots, \tag{21}$$

where $V_{kl}' = \langle\varphi_k| V' |\varphi_l\rangle$ and $E_c = \langle\varphi_c| H_0' |\varphi_c\rangle$. States $|\varphi_i\rangle$ with $i \neq c$ are states where the excitation is absorbed in the ensemble spin i. We note that $V_{\mathrm{cc}}' = 0$ and that $V_{ij}' = 0$ for $i, j \neq c$ since our Hamiltonian does not include spin-spin interaction. Only the second term in Eq. (21) remains and we can write

$$R_{\mathrm{cc}}(z) = \sum_{i\neq c} \frac{|g_i|^2}{z - E_i}. \tag{22}$$

Introducing the coupling density profile $\rho(\omega) \equiv \sum_j |g_j|^2 \delta(\omega - \mathrm{Re}\omega_j)$ as it is done in [13] leads to

$$R_{\mathrm{cc}}(z) = \int \frac{\rho(\omega)}{z - \omega + \frac{\mathrm{i}}{2}\gamma_{\mathrm{hom}}} d\omega. \tag{23}$$

Approaching the branch cut at $\omega - \frac{\mathrm{i}}{2}\gamma_{\mathrm{hom}}$ we write

$$\lim_{\eta\to 0^+} R_{\mathrm{cc}}\left(\omega - \frac{\mathrm{i}}{2}\gamma_{\mathrm{hom}} \pm i\eta\right) = R_{\mathrm{cc}}^{\pm}\left(\omega - \frac{\mathrm{i}}{2}\gamma_{\mathrm{hom}}\right). \tag{24}$$

Using $\lim_{\eta\to 0^+} \frac{1}{x \pm \mathrm{i}\eta} = \mathrm{P}\frac{1}{x} \mp \mathrm{i}\pi\delta(x)$, where P denotes the Cauchy principal value, we find

$$R_{\mathrm{cc}}^{\pm}\left(\omega - \frac{\mathrm{i}}{2}\gamma_{\mathrm{hom}}\right) = \mathrm{P}\int \frac{\rho(\omega')}{\omega - \omega'} d\omega' \mp i\pi\rho(\omega). \tag{25}$$

Experimentally we probe the transmission of a weak probe signal amplitude through the cavity as a function of frequency. The position and shape of the weak-field transmission resonances can be determined from the complex poles of $G_{\mathrm{cc}}^+(\omega) = 1/[\omega - \omega_c - R_{\mathrm{cc}}^+(\omega)]$, which contains the spin energy distribution on the right-hand side. We can therefore extract information about the coupling density $\rho(\omega) = -\frac{1}{\pi}\mathrm{Im}R_{\mathrm{cc}}^+(\omega - \frac{\mathrm{i}}{2}\gamma_{\mathrm{hom}})$ by carefully analyzing the measured transmission spectrum. For small γ_{hom} the reconstruction simplifies to

$$\rho(\omega) \approx -\frac{1}{\pi}\mathrm{Im}R_{\mathrm{cc}}^+(\omega) + \frac{1}{2\pi}\frac{\partial \mathrm{Re}R_{\mathrm{cc}}^+(\omega)}{\partial\omega}\gamma_{\mathrm{hom}}, \tag{26}$$

where $\mathrm{Im}R_{\mathrm{cc}}^+(\omega - \frac{\mathrm{i}}{2}\gamma_{\mathrm{hom}})$ is expanded in a Taylor series around $\gamma_{\mathrm{hom}} = 0$. We can therefore directly use the frequency distribution of the transmitted signal $|\langle a_c\rangle_{\mathrm{st}}|^2$ via

$$|\langle a_c\rangle_{\mathrm{st}}|^2 \propto |G_{\mathrm{cc}}^+(\omega, \omega_c)|^2 = \frac{1}{[\omega - \omega_c - \mathrm{Re}R_{\mathrm{cc}}^+(\omega)]^2 + [\kappa + \mathrm{Im}R_{\mathrm{cc}}^+(\omega)]^2}, \tag{27}$$

to determine $R_{\mathrm{cc}}^+(\omega)$. Let us point out here that Eq. (27) exhibits a Lorentzian shape as a function of ω_c with peak position $\omega - \mathrm{Re}R_{\mathrm{cc}}^+(\omega)$ and peak width of $2[\kappa + \mathrm{Im}R_{\mathrm{cc}}^+(\omega)]$. After extraction of the relevant parameters which determine $R_{\mathrm{cc}}^+(\omega)$ from the measured spectra, we can simply use Eq. (26) to find the coupling density $\rho(\omega)$. Assuming that all spins are coupled with equal strength, one finds that $\rho(\omega) = g^2 N \mathcal{M}(\omega)$ where $\mathcal{M}(\omega)$ is the frequency distribution of the spins.

The shape of the coupling density, i.e., the frequency distribution of the spins, plays an important role in the cavity-ensemble interaction [12,13]. If the coupling density falls off sufficiently fast with distance from the center, the width of the Rabi peaks will decrease with increasing collective coupling strength $g\sqrt{N}$. For the spin frequency distribution, the limiting case is the Lorentzian coupling density profile, for which the

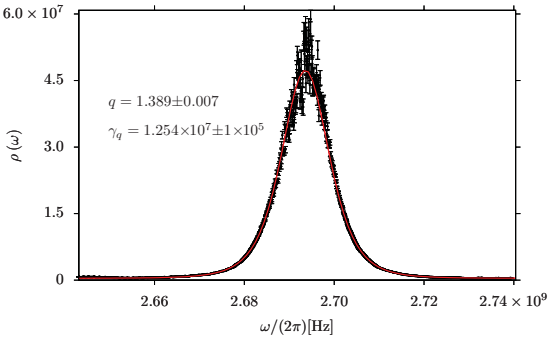

FIG. 4. (Color online) Coupling density of the ensemble determined from an exemplary transmission measurement at $T = 20$ mK. The error bars are calculated from the uncertainties in $R_{cc}^{+}(\omega)$ which we obtain from fitting Eq. (27) to the data. We fit the q Gaussian (red) in Eq. (28) to the coupling density to determine the width and the behavior of the tails of the distribution.

width of the Rabi peaks is independent of $g\sqrt{N}$ [12]. Any distribution falling faster than $1/\omega^2$ will provide a decrease of the width of the Rabi peaks. Moreover, knowing the coupling density gives us the opportunity to study the transmission through the cavity for different parameter ranges via Eq. (20).

To determine $\rho(\omega)$ the raw data have to be rearranged, since in the experiment we cannot simply vary ω_c but we shift the center frequency of the spins by a magnetic field. We therefore shift each scan by $\omega_c - \omega_-^{\mathrm{I}}(B)$ to obtain fixed ensemble frequencies and tuning of the cavity frequency. As the only significant quantity is the detuning between the cavity and the ensemble this does not change the dynamics. For fixed

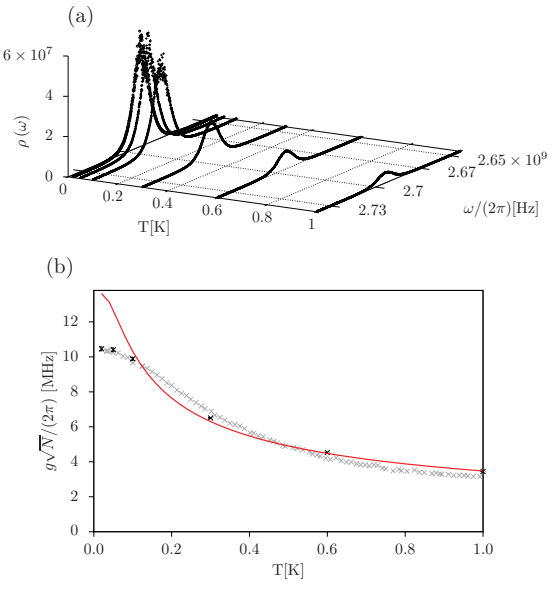

FIG. 5. (Color online) (a) Coupling density for different temperatures. The q parameter and width γ_q of the coupling density do not change significantly with increasing temperature. The coupling $g\sqrt{N} = [\int \rho(\omega) d\omega]^{1/2}$ is reduced, as can be seen in (b). The red line shows $\Omega(T) = a_0\{\tanh[\hbar\omega_-^{\mathrm{I}}/(2k_B T)]\}^{1/2}$ with a_0 chosen to match the high-temperature limit of the data (black markers). To compare $\Omega(T)$ with our previous results determined directly from the splitting we plot the data already shown in Fig. 3 using gray markers.

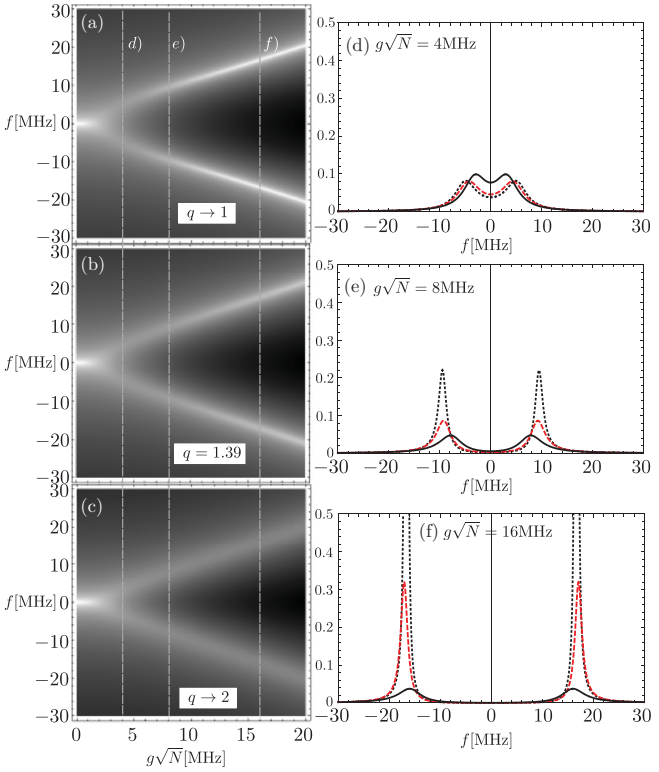

FIG. 6. (Color online) $|G_{cc}(\omega)|^2$ as a function of the collective coupling strength $g\sqrt{N}$ and for three different values of the q-Gaussian parameter q (grayscale figures on the left are plotted on a logarithmic scale). For $g\sqrt{N} = 4, 8$, and 16 MHz, marked by (d), (e), and (f), we show the transmission for all three values of q together. The transmissions for the Gaussian coupling density with $q \to 1$ (dotted black line), for the coupling density of our ensemble with $q = 1.39$ (dashed red line), and for the Lorentzian coupling density with $q \to 2$ (solid black line) are shown on the right. The parameters were chosen to be $\gamma_q/(2\pi) = 10$ MHz, $\kappa/(2\pi) = 0.4$ MHz, and $\gamma_{\mathrm{hom}}/(2\pi) = 1$ Hz.

ω we fit a Lorentzian to $|G_{cc}^{+}(\omega, \omega_c)|^2$ to determine $R_{cc}^{+}(\omega)$ in order to calculate $\rho(\omega)$. We plot an exemplary result for $\rho(\omega)$ in Fig. 4. To determine the behavior of the tails of the distribution we fit the function

$$L(\omega) = b + I\left[1 - (1-q)\frac{(\omega - \omega_0)^2}{a}\right]^{\frac{1}{1-q}} \qquad (28)$$

to the data. $L(\omega)$ is related to the q Gaussian, a Tsallis distribution. The dimensionless parameter $1 < q < 3$ determines how fast the tails of the distribution fall off, while a is related to the width. The actual width (FWHM) is given by $\gamma_q = 2\sqrt{\frac{a(2^q-2)}{2q-2}}$. For $q \to 1$ we recover a Gaussian distribution, while for $q = 2$ we find a Lorentzian distribution. The wings fall off as $1/\omega^{2/(q-1)}$.

From the fit in Fig. 4 we find values for $q = 1.389 \pm 0.007$ and $\gamma_q/(2\pi) = (12.54 \pm 0.10)$ MHz. The temperature during the measurement was 20 mK.

The same analysis is performed for data measured for $T =$ 20–1000 mK [see Fig. 5(a)]. The fitted curves are not shown. For the resulting coupling densities we find almost no change in the width or the q parameter. However, with increasing

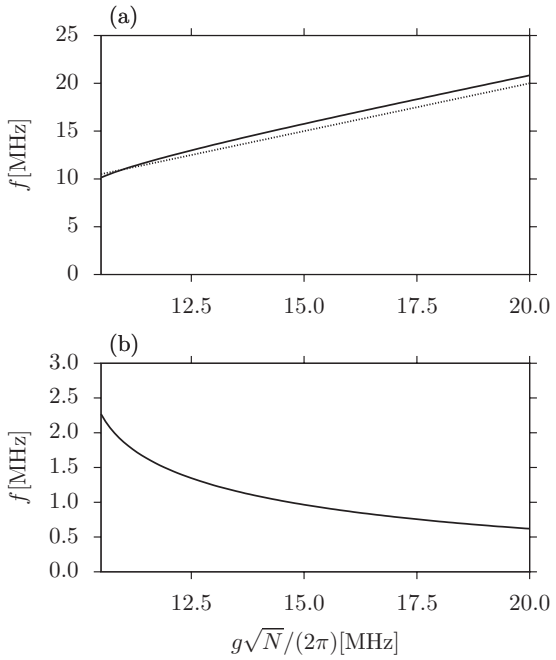

FIG. 7. (a) Real part and (b) modulus of the imaginary part of one of the complex poles of $G^{+}_{cc}(\omega)$ in the regime where $g\sqrt{N}/(2\pi) > \gamma_q/(2\pi) = 10$ MHz. The collective coupling strength $g\sqrt{N}$ is shown as a dotted line in (a). With increasing $g\sqrt{N}$ the modulus of the imaginary part, proportional to the width of the Rabi peaks, is reduced.

temperature $\int \rho(\omega)d\omega = g^2N$ is reduced, as can be seen in Fig. 5(b). The resulting coupling strength is in agreement with the results obtained from the analysis in Sec. III B. It also reproduces the unexpected behavior for small values of T.

To study the behavior of an ensemble following a q-Gaussian distribution with the q parameter we determined, we show $|G_{cc}(\omega)|^2$ for $\omega_c = \omega_0$ as a function of the collective coupling strength $g\sqrt{N}$ in Fig. 6(b). The transmission for an ensemble with Gaussian distribution ($q \to 1$) is shown in Fig. 6(a) and for a Lorentzian distribution ($q \to 2$) is is shown in Fig. 6(c). The width parameter a is chosen accordingly to ensure that γ_q is the same for all three cases. In Figs. 6(d)–6(f) the transmission for the three ensemble types is shown for $g\sqrt{N} = 4,8$, and 16 MHz, respectively. For the ensemble with Lorentzian distribution (solid black line) we see that the width of the Rabi resonances remains constant with increasing collective coupling. For the Gaussian distribution (dotted black line) and the intermediate distribution with $q = 1.39$ (dashed red line) we find a decrease in the peak width for increasing collective coupling. In Fig. 7 we plot the real and imaginary part of one of the complex poles of $G^{+}_{cc}(\omega)$, determining the position and width of one of the Rabi peaks. As we focus on the resonant case the spectrum is symmetric. We chose $\gamma_{hom} = 0$, $\kappa/(2\pi) = 0.4$ MHz, $\gamma_q/(2\pi) = 10$ MHz, and $q = 1.39$. This again shows the decreasing width of the Rabi Peaks as $g\sqrt{N}$ increases.

We therefore assume that for our ensemble it is possible to increase the lifetime of the collective states by increasing the collective coupling. This could be achieved by a further decrease of the mode volume or an increase of the NV density in the sample.

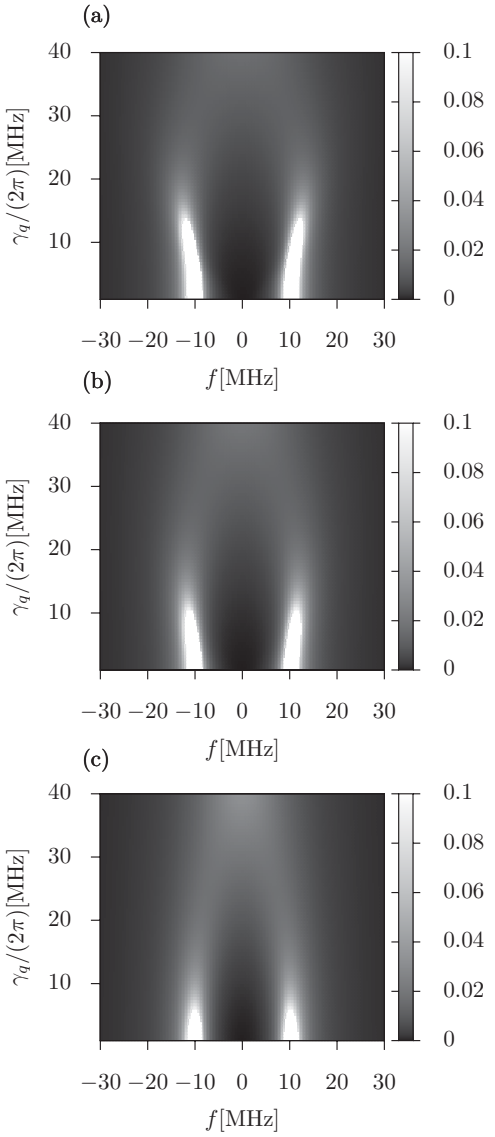

FIG. 8. $|G_{cc}(\omega)|^2$ on resonance as a function of the inhomogeneous width γ_q for an ensemble with (a) Gaussian coupling density, (b) q-Gaussian ($q = 1.39$) coupling density, and (c) Lorentzian coupling density. To keep the transmission visible for large values of γ_q the range of the color coding is limited to [0,0.1]. The parameters were chosen to be $g\sqrt{N}/(2\pi) = 10$ MHz, $\kappa/(2\pi) = 0.4$ MHz, and $\gamma_{hom}/(2\pi) = 1$ Hz.

In Fig. 8 we show the behavior of the transmission with increasing γ_q. For the Lorentzian coupling density the splitting of the resonance peaks is always reduced if $\gamma_q > 0$. For coupling densities falling off faster than $1/\omega^2$, as is the case in Figs. 8(a) and 8(b), the splitting of the resonance peaks is even slightly increased for $\gamma_q > 0$, until the peaks finally merge. Hence a finite but small enough inhomogeneous width might even mimic somewhat higher active spin numbers.

As a bottom line we see that common coupling to a cavity mode can suppress dephasing of the polarization, if the effective Rabi frequency is larger than the inhomogeneous width. This could be interpreted as the effect that the exchange of the excitation between the ensemble and the cavity is so fast that there is no time for decoherence in the ensemble.

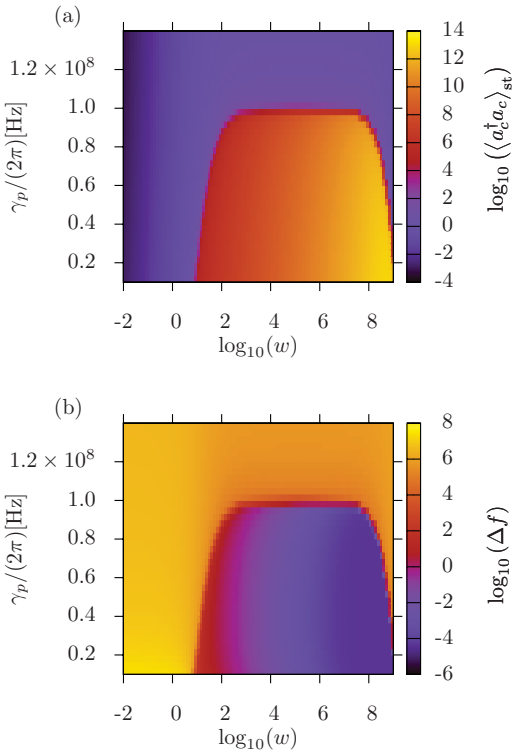

FIG. 9. (Color online) (a) Steady-state number of photons in the cavity $\langle a_c^\dagger a_c \rangle_{\rm st}$ as a function of the incoherent pump rate w and the inhomogeneous width γ_p. The resulting linewidth Δf is shown in (b). For small γ_p both Δf and $\langle a_c^\dagger a_c \rangle_{\rm st}$ show rapid changes as w becomes larger than $\gamma_{\rm hom}$. The critical width of the inhomogeneity is given by $\gamma_{p,\rm crit} = g^2 N/\kappa$. The parameters were chosen to be $N = 10^{12}$, $g/(2\pi) = 10$ Hz, $\kappa/(2\pi) = 1$ MHz, and $\gamma_{\rm hom}/(2\pi) = 1$ Hz.

IV. TRANSMISSION LINE MICROMASER WITH AN INHOMOGENEOUS NV ENSEMBLE

A recent proposal to construct a laser operating on an ultranarrow atomic clock transition predicted very narrow optical emission above threshold [17]. Similar ideas, employing the collective coupling between a cold atomic ensemble and a microwave cavity, have been proposed to construct stable stripline oscillators in the microwave regime [18].

Here we study the prospects of implementing such an oscillator by coupling a diamond to the CPW resonator. At first sight in view of the MHz scale inhomogeneous broadening, one would expect fast dephasing. However, as we have seen above, for strong enough coupling one observes a continuous rephasing of the polarization inducing a long lived polarization and coherent Rabi oscillations. Thus one could expect narrow microwave emission nevertheless.

Let us consider the case of the cavity mode tuned to resonance with the spin transition $|0\rangle_{\rm I} \to |-\rangle_{\rm I}$, which is partially inverted by an external incoherent pump. Such a pump could in principle be facilitated by optical pumping and it can be consistently modeled by a reversed spontaneous decay. Alternatively one could think of pulsed inversion by tailored microwave pulses or a time switching of the magnetic bias field.

Mathematically such incoherent pumping can be modeled by adding the terms $-\frac{w}{2}\sum_{j=1}^{N}(\sigma_j^-\sigma_j^+\rho + \rho\sigma_j^-\sigma_j^+ - 2\sigma_j^+\rho\sigma_j^-)$, where w denotes the pump rate, to the Liouvillian in Eq. (9).

For the explicit calculations, here we use the effective linewidth model, as outlined in Sec. III B without any coherent pump. Hence the total phase symmetry of the system is not broken and we assume $\langle a_c \rangle = \langle a_c^\dagger \rangle = \langle \sigma_j^\pm \rangle = 0$. Starting from the master equation in Eq. (8) we derive four coupled equations for $\langle \sigma_j^z \rangle$, $\langle a_c^\dagger a_c \rangle$, $\langle a_c \sigma_i^+ \rangle$, and $\langle \sigma_i^+ \sigma_j^- \rangle$. We used the cumulant expansion $\langle a_c^\dagger a_c \sigma_i^z \rangle = \langle a_c^\dagger a_c \sigma_i^z \rangle_{\rm cum} + \langle a_c^\dagger a_c \rangle \langle \sigma_i^z \rangle$, which takes this simple form because of the total phase invariance. Assuming that the higher-order cumulant $\langle a_c^\dagger a_c \sigma_i^z \rangle_{\rm cum}$ can be neglected, we arrive at a closed set of four equations that can be solved analytically. To study the spectrum of the emitted light we calculate the two-time correlation function $\langle a_c^\dagger(\tau) a_c(0) \rangle$ via the quantum regression theorem. We switch to a frame rotating with ω_c and define $\Delta = \omega_-^{\rm I} - \omega_c$. We obtain

$$\frac{d}{d\tau}\begin{pmatrix} \langle a_c^\dagger(\tau)\, a_c(0)\rangle \\ \langle \sigma_i^+(\tau) a_c(0)\rangle \end{pmatrix} = \begin{pmatrix} -\kappa & igN \\ -ig\langle \sigma_i^z \rangle_{\rm st} & -\left[\frac{w+\gamma_{\rm hom}}{2} + \gamma_{\rm hom}\bar{n}(T,\omega_-^{\rm I}) + \gamma_p - i\Delta\right] \end{pmatrix} \begin{pmatrix} \langle a_c^\dagger(\tau)\, a_c(0)\rangle \\ \langle \sigma_i^+(\tau)\, a_c(0)\rangle \end{pmatrix}. \tag{29}$$

From Eq. (29) we can calculate the spectrum via Laplace transformation [20]. We show the linewidth of the obtained spectrum in the resonant case ($\Delta = 0$) for different values of the pump w and the inhomogeneous width γ_p (see Fig. 9). The minimum linewidth is $\Delta f \approx g^2/\kappa$. For small γ_p the region where we find narrow linewidth emission is characterized by $\gamma_{\rm hom} < w < 2g^2 N/\kappa$. The critical width of the inhomogeneity is given by $\gamma_{p,\rm crit} = g^2 N/\kappa$. Hence once we achieve enough pumping and coupling strength the system could provide for an extremely stable microwave oscillator.

V. CONCLUSIONS

We showed theoretically and experimentally that an ensemble of spins with an inhomogeneous frequency distribution coupled to a cavity mode can exhibit strong coupling, where the coherent energy exchange between mode and ensemble dominates cavity decay and polarization dephasing. A detailed theoretical modeling connecting probe transmission and frequency distribution allows us to extract not only the effective coupling strength and particle number but also the detailed frequency distribution. The microscopic mechanisms that cause the inhomogeneous broadening are not treated

as a central theme in this work, but we hope that the knowledge of the frequency distribution can be of use in further investigations on this subject. Interestingly for our dense NV ensemble, the frequency distribution of the spins can be well described as a q Gaussian with $q = 1.39$, showing that the wings of the distribution fall off faster than $1/\omega^2$. The temperature dependence of the effective available spin number fits quite well with expectations, except for an unexpected decrease for very low temperature. In summary such an NV ensemble-cavity QED system exhibits a prolonged lifetime of the eigenstates of the coupled cavity-ensemble system [13] and has great potential as a quantum interface between superconducting and optical qubits. The long effective T_1 time could also be the basis of building a compact ultrastable microwave oscillator if the strong coupling overcomes the dephasing from the inhomogeneous broadening.

ACKNOWLEDGMENTS

We thank Klaus Mølmer for his helpful remarks and open discussions. K. S. was supported by the DOC-fFORTE doctoral program. R. A. and T. N. were supported by CoQuS. C. K. was supported by FunMat. We acknowledge support by the Austrian Science Fund through Project No. SFB F40.

[1] D.F. Phillips, A. Fleischhauer, A. Mair, R.L. Walsworth, and M.D. Lukin, Phys. Rev. Lett. **86**, 783 (2001).
[2] J. Taylor, P. Cappellaro, L. Childress, L. Jiang, D. Budker, P. Hemmer, A. Yacoby, R. Walsworth, and M. Lukin, Nature Physics **4**, 810 (2008).
[3] J. Verdú, H. Zoubi, C. Koller, J. Majer, H. Ritsch, and J. Schmiedmayer, Phys. Rev. Lett. **103**, 043603 (2009).
[4] P. Rabl, D. DeMille, J.M. Doyle, M.D. Lukin, R.J. Schoelkopf, and P. Zoller, Phys. Rev. Lett. **97**, 033003 (2006).
[5] P. Bushev, A. K. Feofanov, H. Rotzinger, I. Protopopov, J. H. Cole, C. M. Wilson, G. Fischer, A. Lukashenko, and A.V. Ustinov, Phys. Rev. B **84**, 060501 (2011).
[6] Y. Kubo *et al.*, Phys. Rev. Lett. **105**, 140502 (2010).
[7] R. Amsüss, Ch. Koller, T. Nöbauer, S. Putz, S. Rotter, K. Sandner, S. Schneider, M. Schramböck, G. Steinhauser, H. Ritsch, J. Schmiedmayer, and J. Majer, Phys. Rev. Lett. **107**, 1 (2011).
[8] F. Jelezko and J. Wrachtrup, Phys. Status Solidi A **203**, 3207 (2006).
[9] L. Childress, M. Gurudev Dutt, J. Taylor, A. Zibrov, F. Jelezko, J. Wrachtrup, P. Hemmer, and M. Lukin, Science **314**, 281 (2006).
[10] V. Acosta *et al.*, Phys. Rev. B **80**, 115202 (2009).
[11] R. Houdré, R.P. Stanley, and M. Ilegems, Phys. Rev. A **53**, 2711 (1996).
[12] I. Diniz, S. Portolan, R. Ferreira, J. M. Gérard, P. Bertet, and A. Auffèves, Phys. Rev. A **84**, 063810 (2011).
[13] Z. Kurucz, J.H. Wesenberg, and K. Mølmer, Phys. Rev. A **83**, 053852 (2011).
[14] D. Braun, J. Hoffman, and E. Tiesinga, Phys. Rev. A **83**, 062305 (2011).
[15] H. Carmichael, *An Open Systems Approach to Quantum Optics: Lectures Presented at the Université Libre de Bruxelles, October 28 to November 4, 1991* (Springer, New York, 1993), Vol. 18.
[16] R. Kubo, J. Phys. Soc. Jpn. **17**, 1100 (1962).
[17] D. Meiser, J. Ye, D. R. Carlson, and M. J. Holland, Phys. Rev. Lett. **102**, 163601 (2009).
[18] K. Henschel, J. Majer, J. Schmiedmayer, and H. Ritsch, Phys. Rev. A **82**, 033810 (2010).
[19] C. Cohen-Tannoudji, J. Dupont-Roc, and G. Grynberg, *Atom-Photon Interactions: Basic Processes and Applications* (John Wiley and Sons Inc., New York, 1992).
[20] P. Meystre and M. Sargent, *Elements of Quantum Optics* (Springer-Verlag, New York, 2007).